Electronic Supplementary Information for:

Photo-induced Electron Transfer in a Diamino-substituted $Ru(bpy)_3[PF_6]_2$ Complex and Its Application as Triplet Photosensitizer for Nitric Oxide (NO)-Activated Triplet-Triplet Annihilation Upconversion

Kejing Xu,[a] Jianzhang Zhao*[a] and Evan G. Moore*[b]

[a] State Key Laboratory of Fine Chemicals, School of Chemical Engineering, Dalian University of Technology, Dalian 116024 (China)

E-mail: zhaojzh@dlut.edu.cn Web: http://finechem2.dlut.edu.cn/photochem

[b] School of Chemistry and Molecular Biosciences, University of Queensland, St Lucia Campus, Brisbane, QLD, 4072, Australia. Phone: Int. +61 7 3365 3862 Fax: Int. +61 7 3365 4273 Email: egmoore@uq.edu.au

Index

1.0 Synthesis of Ru-1 and Ru-2

Scheme S1. Synthesis of Ru-1 and Ru-2 [a]

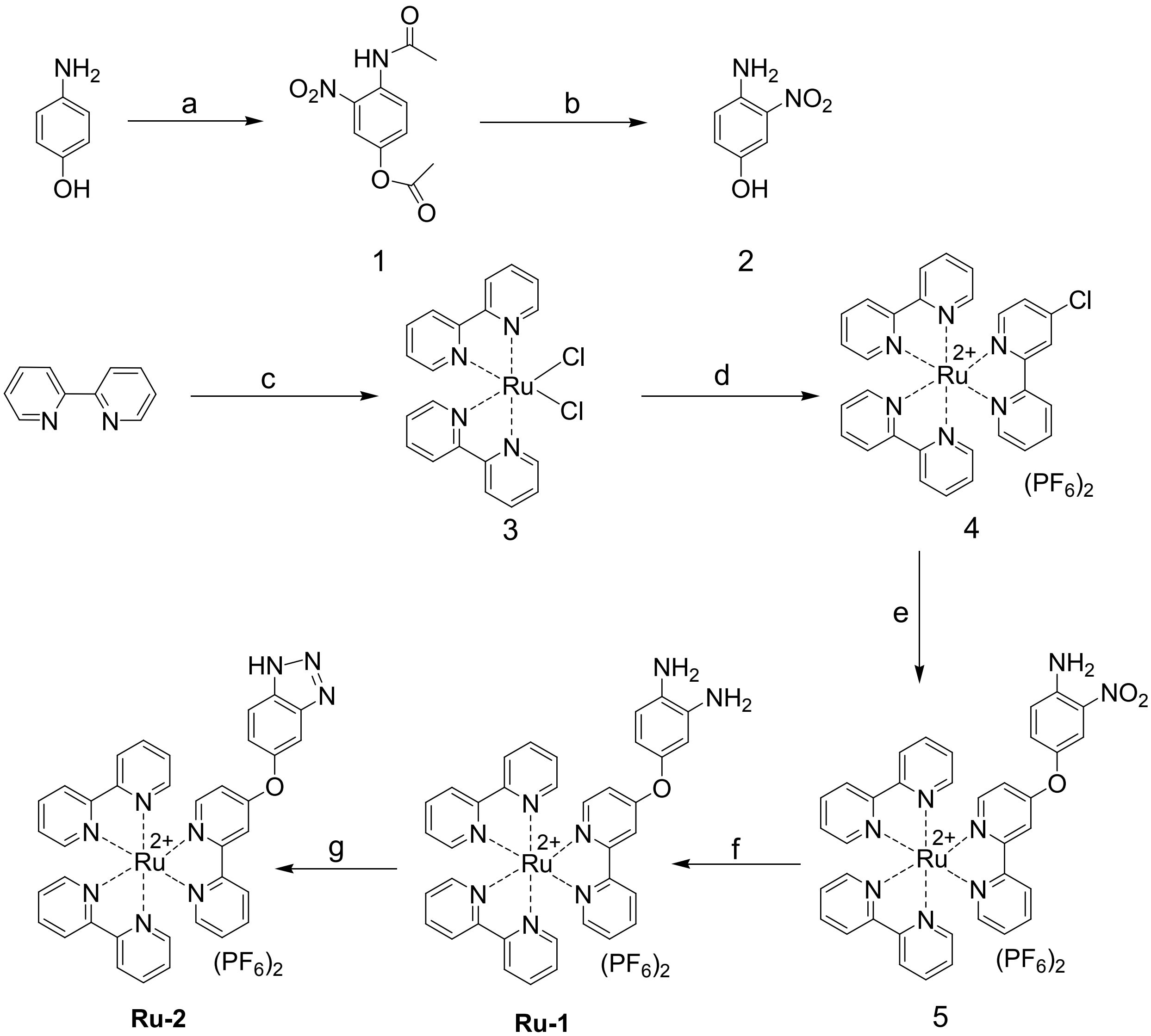

[a] Key: (a) acetic anhydride, Fuming nitric acid, 1.5 h. Yield: 81%; (b) NaOH, ethanol, 60 °C, 1 h. Yield: 49%; (c) LiCl, DMF, 160 °C, 8 h. Yield: 42%; (d) methanol, reflux, 8 h. Yield: 83%; (e) NaH, dry CH_3CN, r.t. Yield: 95%; (f) hydrazine hydrate, Pd/C, ethanol, reflux, 2 h. Yield: 96%; (g) $NaNO_2$, 2 M HCl, 0 °C, 2 h. Yield: 69%.

Synthesis of Compound 2

2: The compound **1** and compound **2** was synthesized according to the literature report.[1] Compound 2: (Yield: 49.0 %). mp 149.2– 150.4 °C. ^{1}H NMR (400 MHz, $CDCl_3$): δ 7.57 (d, 1H, J = 4.0 Hz), 7.04 (m, 1H), 6.76 (d, 1H, J = 12.0 Hz), 5.81 (s, 2H), 4.98 (s, 1H). MALDI-HRMS: calcd ($[C_6H_6N_2O_3]^+$), m/z = 154.0378, found m/z = 154.0379.

Synthesis of Compound 2

3:[2] Yield: 41.6%. ^{1}H NMR (400 MHz , DMSO-d6): δ(ppm) 9.98 (d, 2H, *J* = 5.0 Hz), 8.64 (d, 2H, *J* = 10.0 Hz), 8.49 (d, 2H, *J* = 10.0 Hz), 8.07–8.04 (m, 2H), 7.76 (t, 2H, *J* = 5.0 Hz), 7.69–7.65 (m, 2H), 7.51 (d, 2H, *J* = 5.0 Hz), 7.11–7.09 (m, 2H). ESI-MS (m/z): calcd ($[C_{20}H_{16}N_4Cl_2Ru + Na]^+$), *m/z* = 506.9693, found *m/z* = 506.9702.

Synthesis of Compound 4

4:[3] Yield: 83%. ^{1}H NMR (400 MHz, CD_3CN): δ 8.58 (d, 1H, *J* = 4.0 Hz), 8.51–8.48 (m, 5H), 8.09–8.03 (m, 5H), 7.78–7.70 (m, 5 H), 7.65 (d, 1H, *J* = 4.0 Hz), 7.44–7.39 (m, 6H); ESI-MS (m/z): calcd ($[M - 2PF_6]^{2+}$), *m/z* = 302.0358, found *m/z* = 302.0365.

Synthesis of Compound 5

5:[3] Yield: 95%. ^{1}H NMR (400 MHz, CD_3CN): δ 8.51–8.47 (m, 4 H), 8.41 (d, 1H, *J* = 12.0 Hz), 8.09–7.97 (m, 6H), 7.90 (d, 1H, *J* = 4.0 Hz), 7.83 (d, 1H, *J* = 4.0 Hz), 7.76–7.71 (m, 4H), 7.50–7.35 (m, 6H), 7.28–7.25 (m, 1H), 7.11 (d, 1H, *J* = 8.0 Hz), 6.93–6.91 (m, 1H), 6.65 (s, 2H); ESI-MS (m/z): calcd ($[M - 2PF_6]^{2+}$), *m/z* = 361.0664, found *m/z* = 361.0657.

Synthesis of Ru-1

Ru-1:[3] Yield: 95.7%. ^{1}H NMR (400 MHz, CD_3CN): δ 8.50–8.46 (m, 4 H), 8.37 (d, 1H, *J* = 8.0 Hz), 8.08–7.99 (m, 6H), 7.83 (d, 1H, *J* = 4.0 Hz), 7.76–7.70 (m, 4H), 7.43–7.35 (m, 6H), 6.82–6.80 (m, 1H), 6.69 (d, 1H, *J* = 8.0 Hz), 6.43 (d, 1H, *J* = 4.0 Hz), 6.34–6.32 (m, 1H), 3.92 (br, 4H); ESI-MS (m/z): calcd ($[M - PF_6]^+$), *m/z* = 837.1228, found *m/z* = 837.1242.

Synthesis of Ru-2

Ru-2:[3] Yield: 69.0 %. ^{1}H NMR (400 MHz, CD_3CN): δ 8.53–8.49 (m, 4 H), 8.38 (d, 1H, *J* = 8.0 Hz), 8.10–7.99 (m, 7H), 7.87 (d, 1H, *J* = 4.0 Hz), 7.78–7.73 (m, 5H), 7.54 (d, 1H, *J* = 8.0 Hz), 7.48–7.37 (m, 5H), 7.32–7.29 (m, 1H), 6.67–6.94 (m, 1H); ESI-MS (m/z): calcd ($[M- 2PF_6]^{2+}$), *m/z* = 351.5691, found *m/z* = 351.5679.

1 H. Yu, Y. Yan, Y. Cai and Y. Gu, *Fine Chemical Intermediates*, 2008, **38**, 40–42.

2 K. Adamson, C. Dolan, N. Moran, R. J. Forster and T. E. Keyes, *Bioconjug. Chem.*, 2014, **25**, 928–944.

3 R. Zhang, Z. Ye, G. Wang, W. Zhang and J. Yuan, *Chem. Eur. J.*, **2010**, *16*, 6884–6891.

2.0 NMR and HR-MS spectra

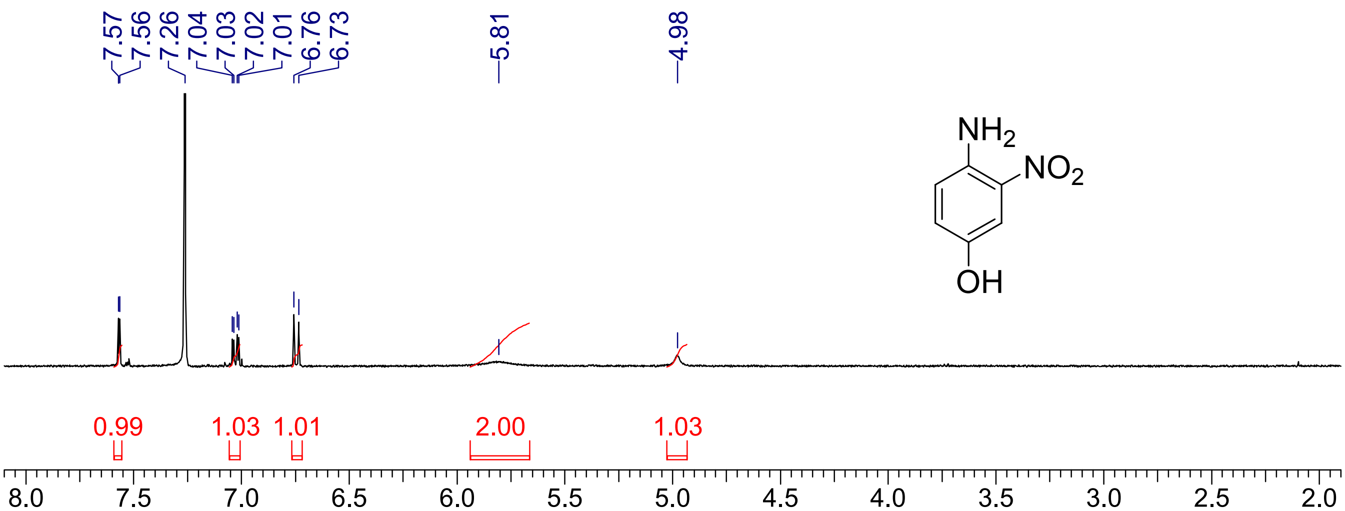

Fig. S1 ^{1}H NMR of compound **2** (400 MHz, $CDCl_3$).

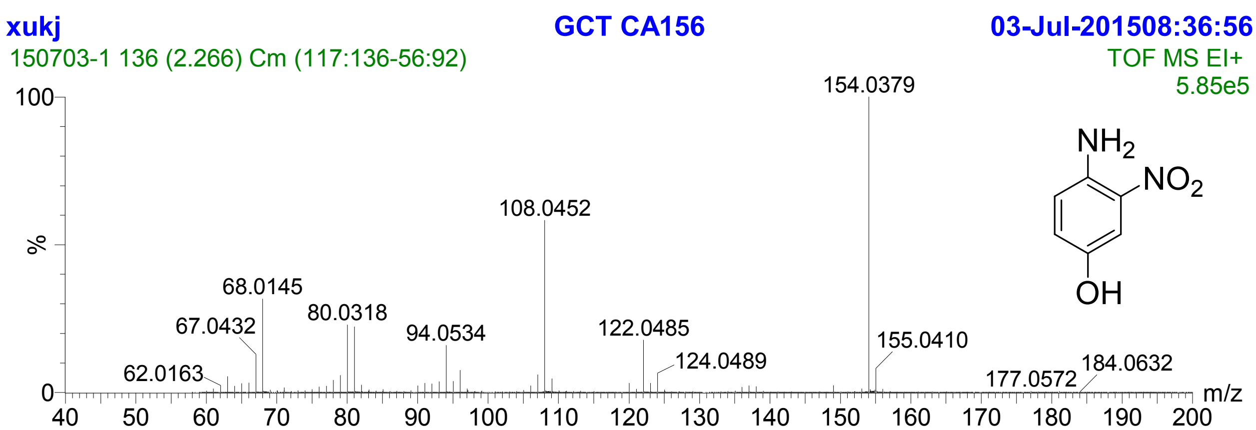

Fig. S2 TOF EI MS of compound **2**.

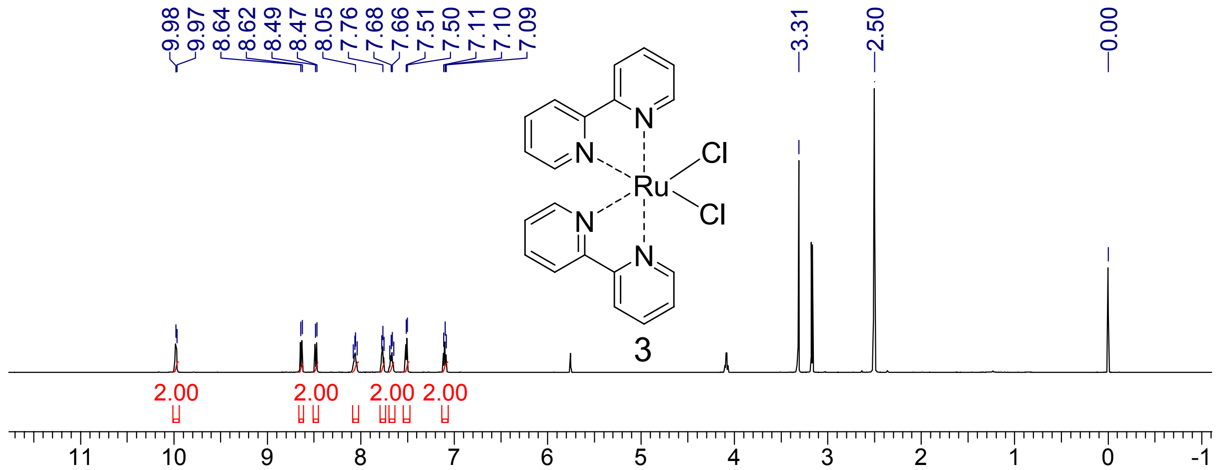

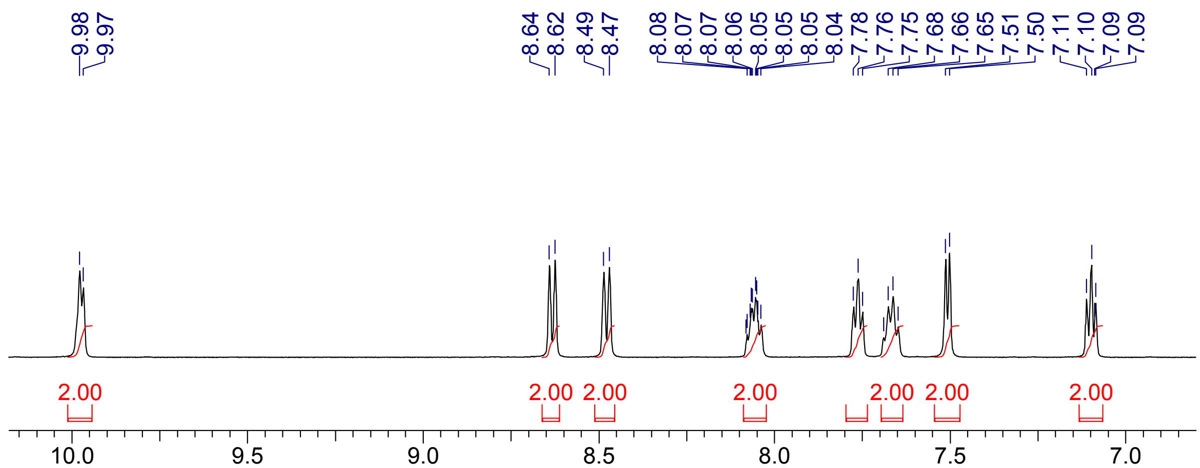

Fig. S3 [1]H NMR of compound **3** (400 MHz, DMSO-d_6).

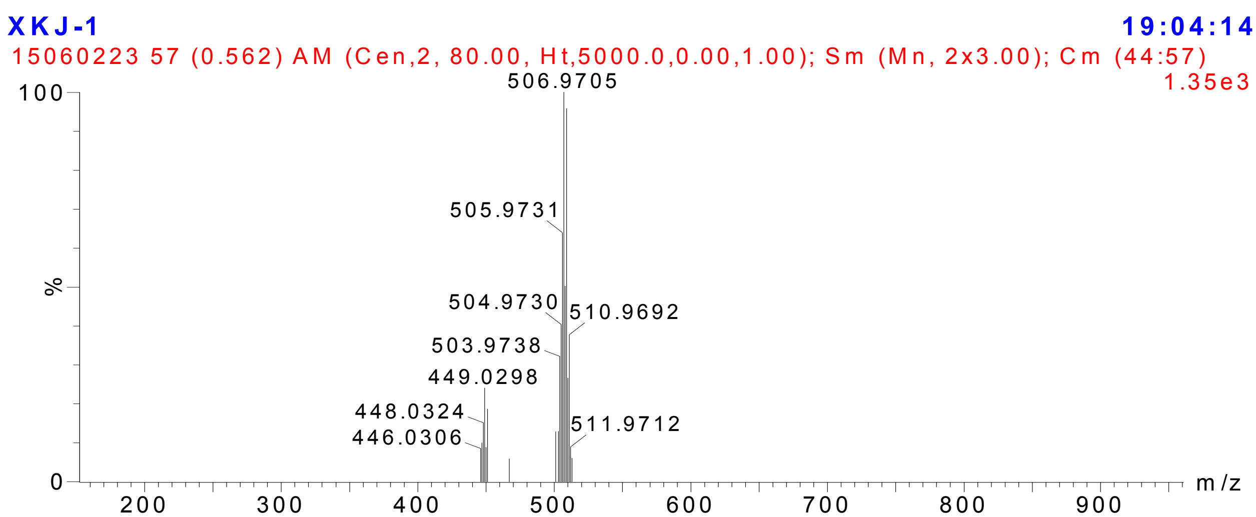

Fig. S4 MALDI-HRMS of compound **3**.

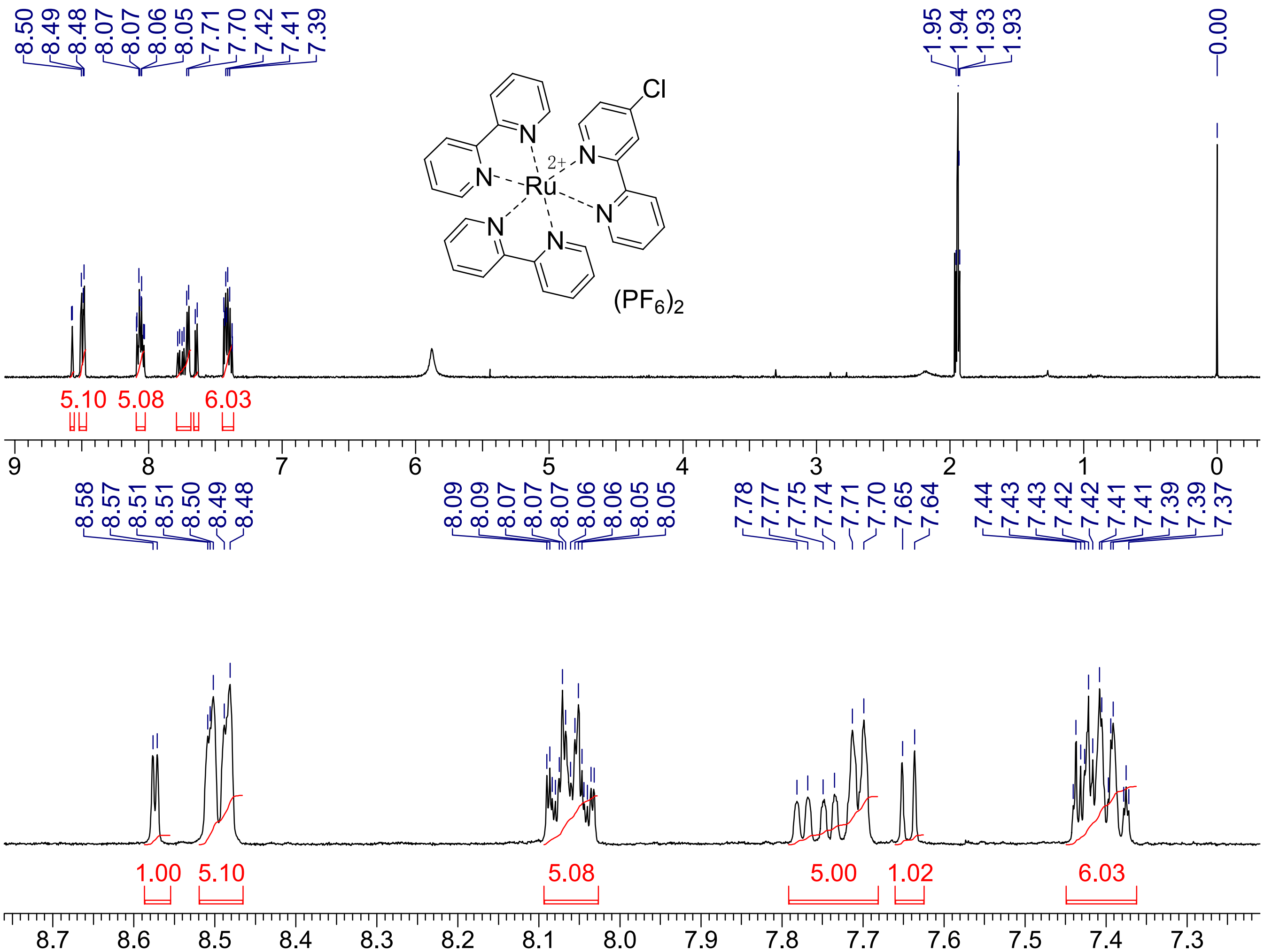

Fig. S5 ^{1}H NMR of compound **4** (400 MHz, CD_3CN).

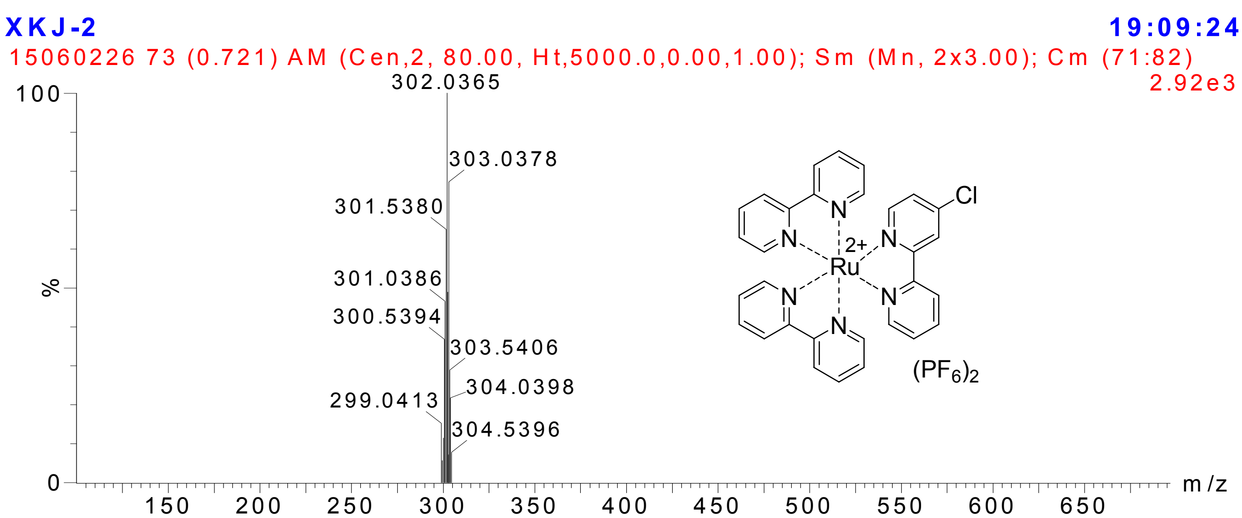

Fig. S6 MALDI-HRMS of compound **4**.

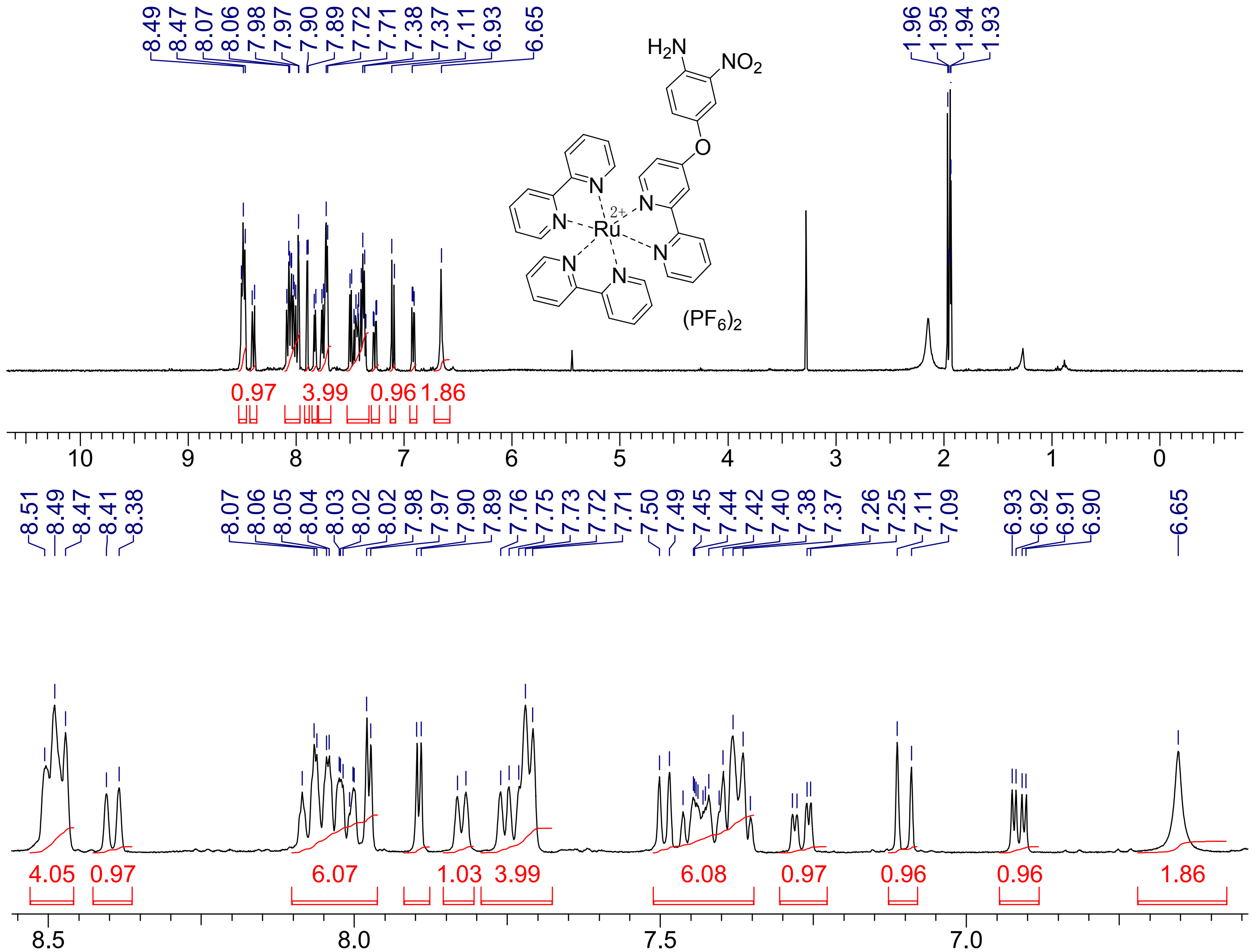

Fig. S7 ^{1}H NMR of compound **5** (400 MHz, CD_3CN).

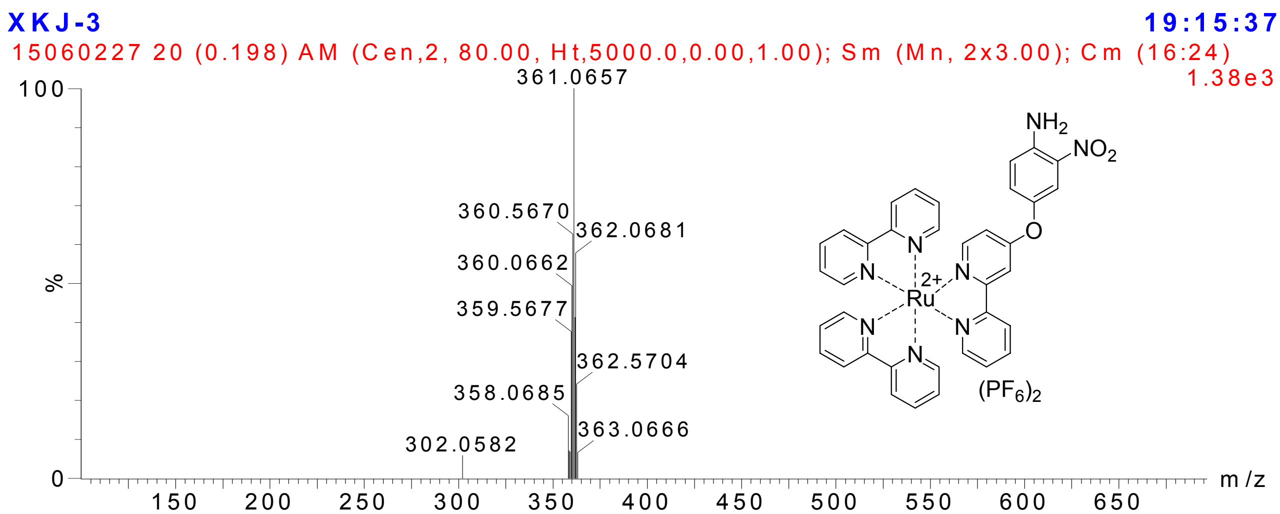

Fig. S8 MALDI-HRMS of compound **5**.

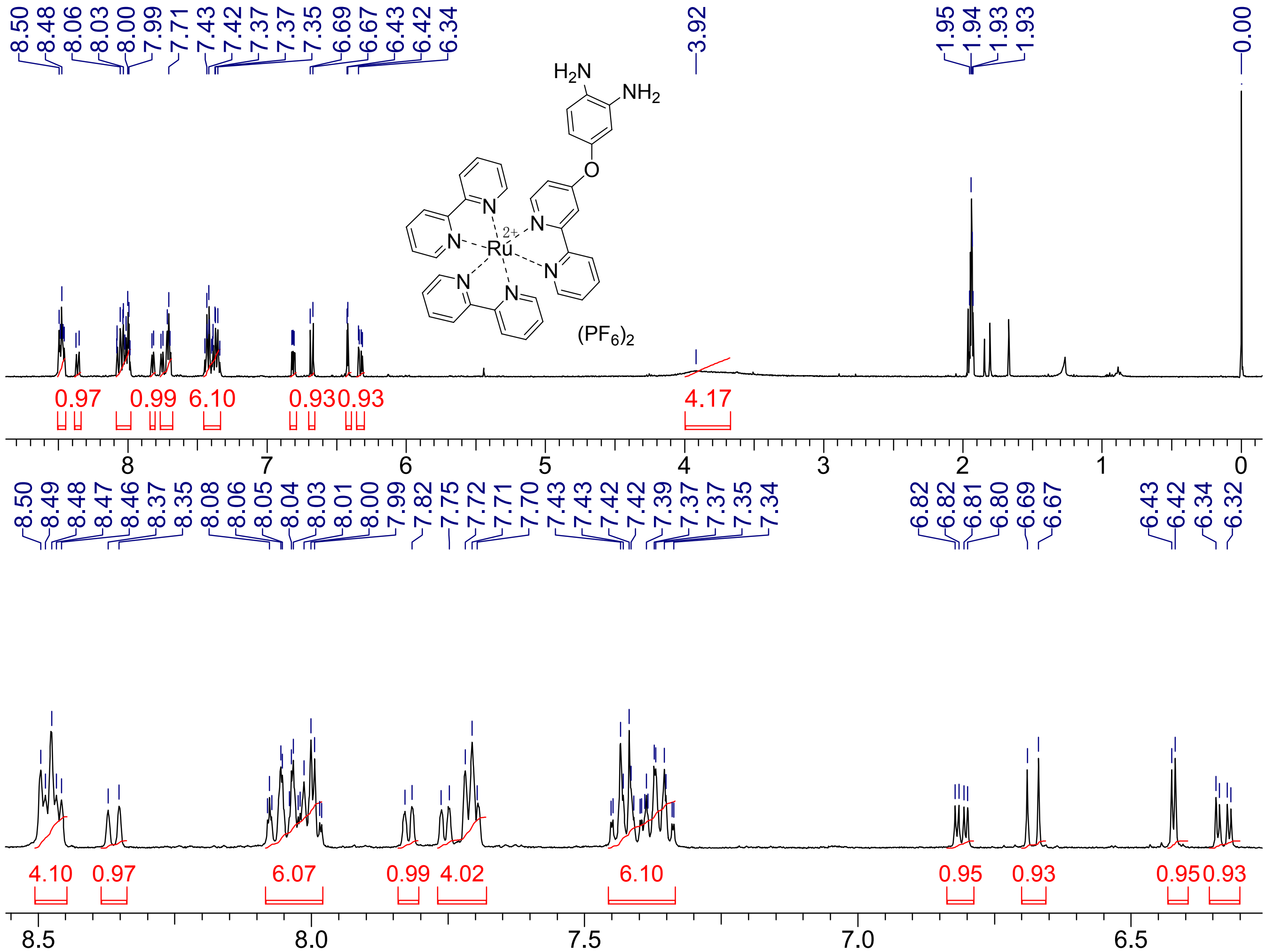

Fig. S9 ^{1}H NMR of **Ru-1** (400 MHz, CD_3CN).

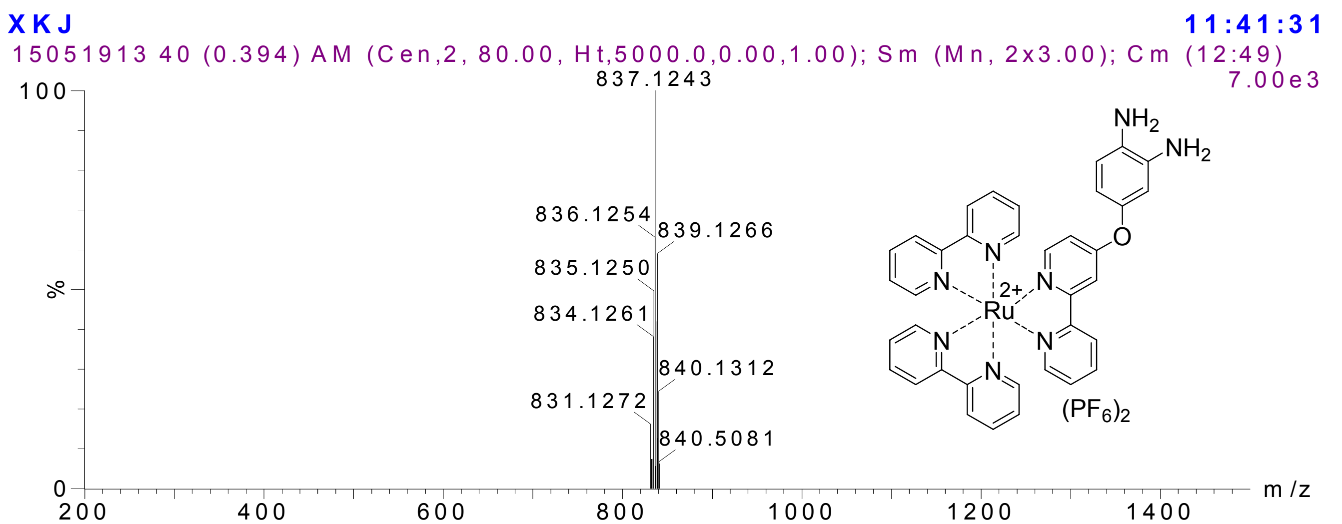

Fig. S10 MALDI-HRMS of **Ru-1**.

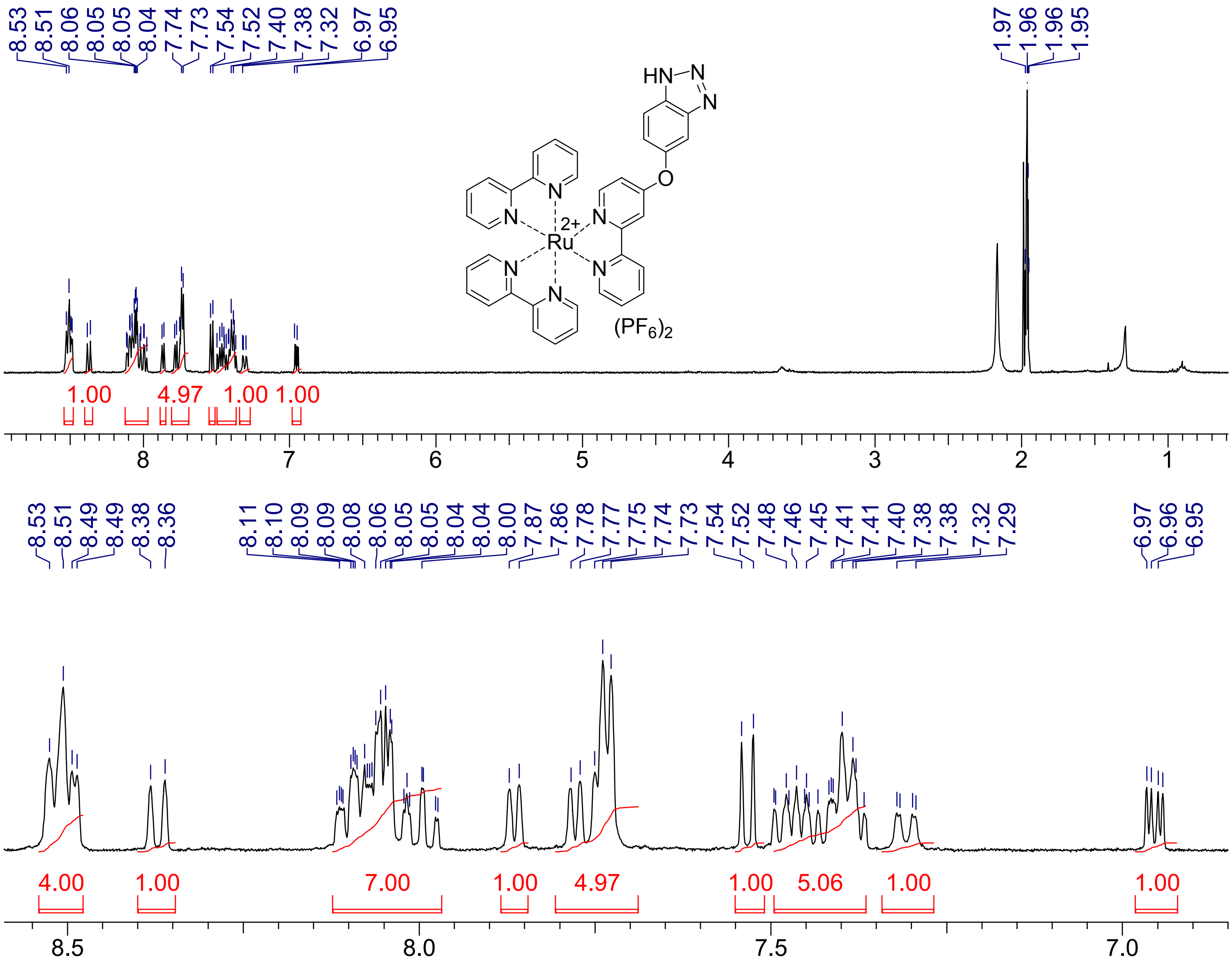

Fig. S11 ^{1}H NMR of **Ru-2** (400 MHz, CD_3CN).

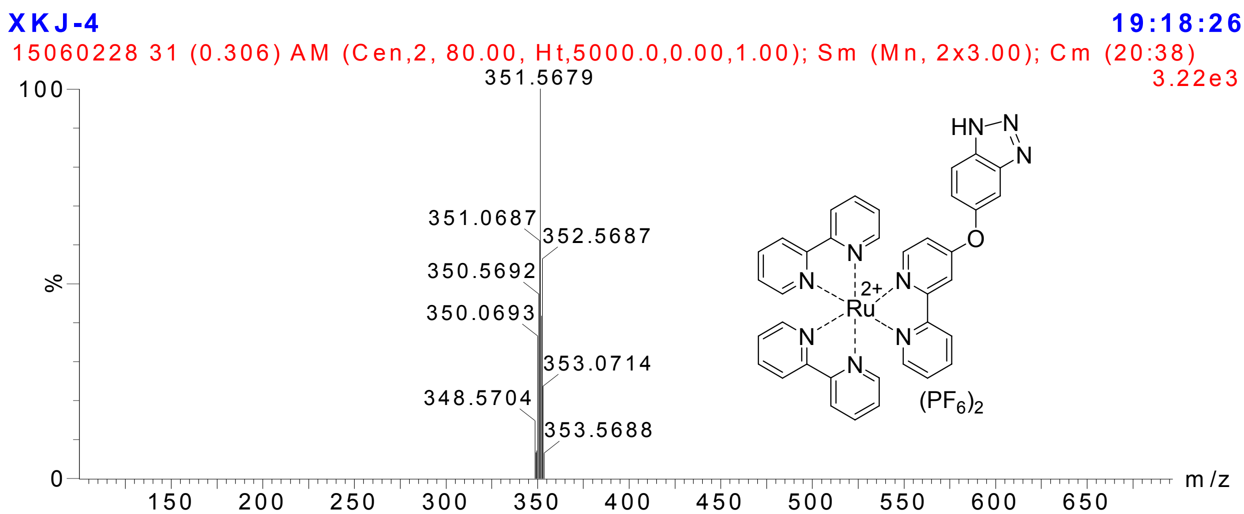

Fig. S12 MALDI-HRMS of **Ru-2**.

3.0 Changes of phosphorescence spectra of Ru-1 upon the addition of NO

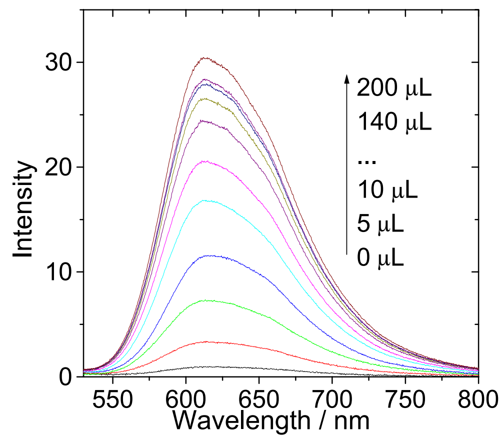

Fig. S13 Changes of phosphorescence spectra of **Ru-1** upon the addition of NO (saturated solution in CH_3CN). $c = 1.0 \times 10^{-5}$ M, $\lambda_{ex} = 445$ nm, In deaerated CH_3CN, 20 °C.

4.0 Phosphorescence emission spectra of Ru-1 and Ru-2 in different deaerated solvents

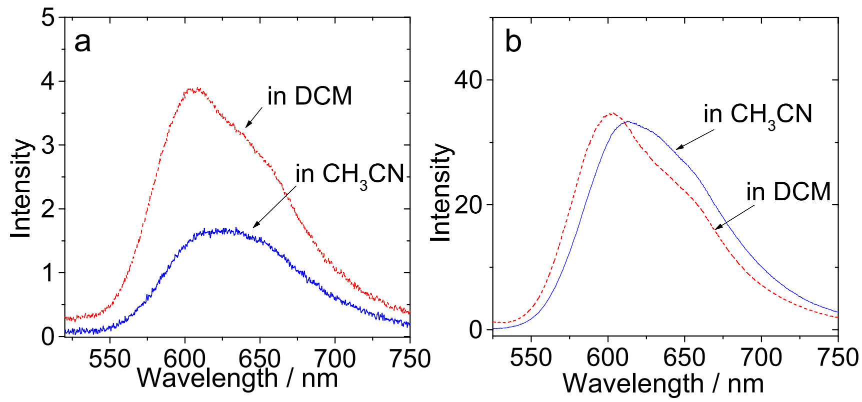

Fig. S14 Phosphorescence emission spectra of **Ru-1** (a) and **Ru-2** (b) in different deaerated solvents. $\lambda_{ex} = 445$ nm, 20 °C, optically matched solution was used ($A = 0.14$).

5.0 Emission spectra and the decay trace of Ru-1 and Ru-2 at 77 K

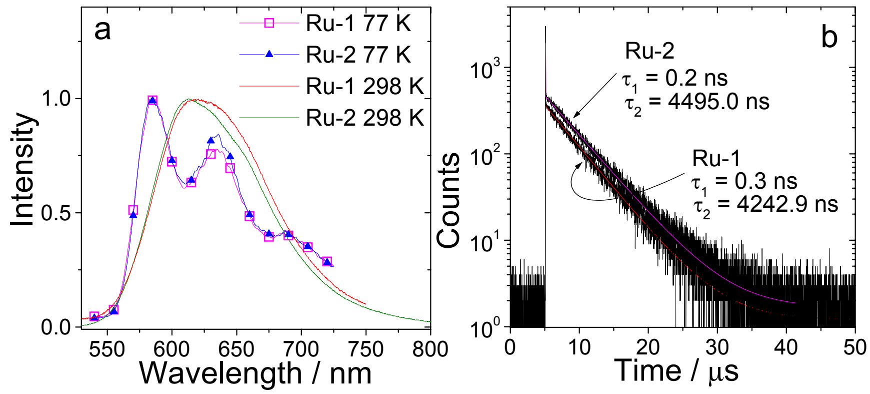

Fig. S15 (a) Normalized emission spectra of **Ru-1** and **Ru-2** at 77 K (in deaerated EtOH–MeOH, 4: 1, v/ v) and 298 K (in deaerated CH_3CN); (b) The lifetime of **Ru-1** and **Ru-2** at 77 K in deaerated EtOH– MeOH (4: 1, v/ v). c = 1.0 × 10 $^{-5}$ M, λ_{ex} = 405 nm, λ_{em} = 585 nm.

6.0 Transient absorption spectra of Ru-1 with a high concentration

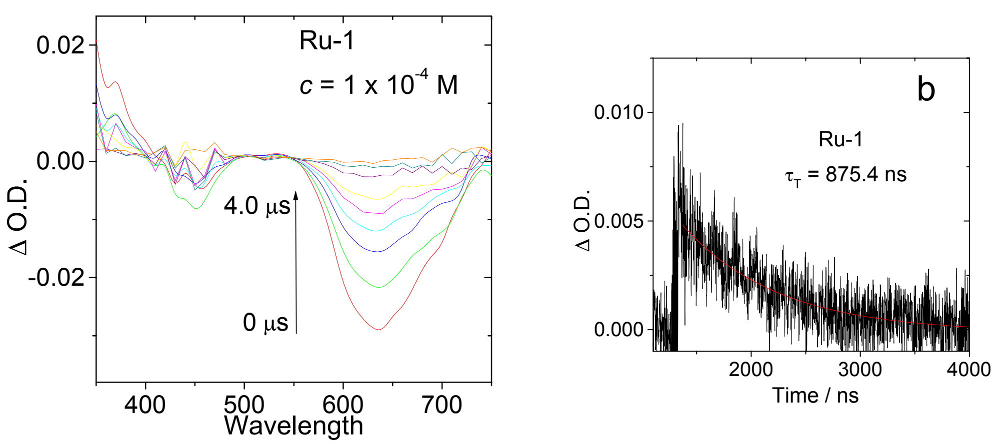

Fig. S16 Transient absorption spectra of **Ru-1**. c [**Ru-1**] = 1.0 × 10^{-4} M. In deaerated CH_3CN. λ_{ex} = 445 nm, 20 °C.

7.0 Nanosecond transient absorption spectra of Ru-1, Ru-2 and Ru(bpy)$_3$

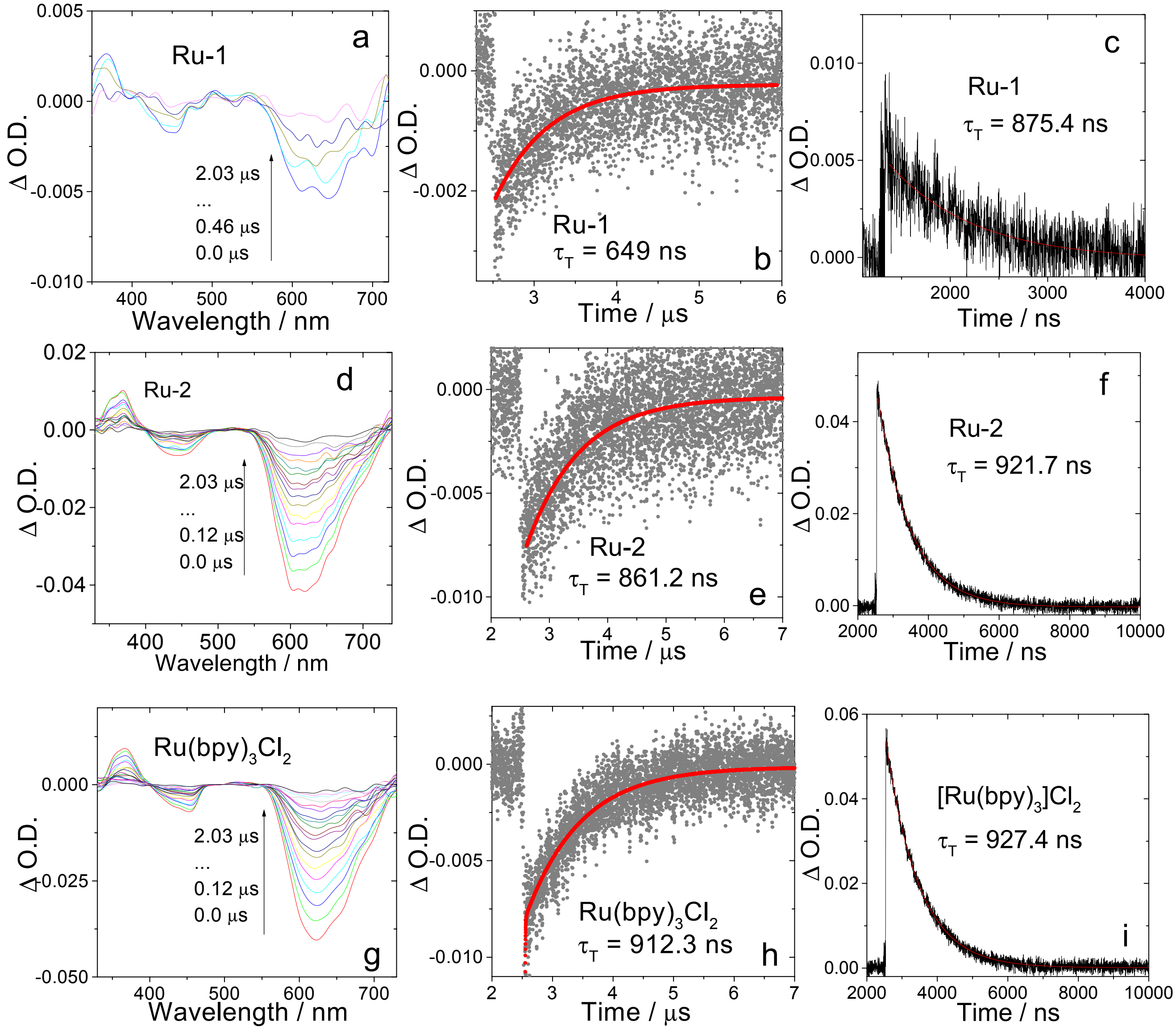

Fig. S17 Transient absorption spectra of the complexes. (a) **Ru-1** and (b) Decay curves of **Ru-1** at 450 nm; (c) Decay curves of **Ru-1** at 610 nm; (d) **Ru-2** and (e) Decay curves of **Ru-2** at 450 nm; (f) Decay curves of **Ru-2** at 610 nm; (g) **Ru(bpy)$_3$Cl$_2$**; (h) Decay curves of **Ru(bpy)$_3$Cl$_2$** at 450 nm; (i) Decay curves of **Ru(bpy)$_3$Cl$_2$** at 610 nm. *c* [Complexes] = 1.0 × 10^{-5} M. In deaerated CH_3CN. λ_{ex} = 445 nm, 20 °C.

8.0 Femtosecond Transient absorption spectra of Ru-2 and Ru(bpy)$_3$

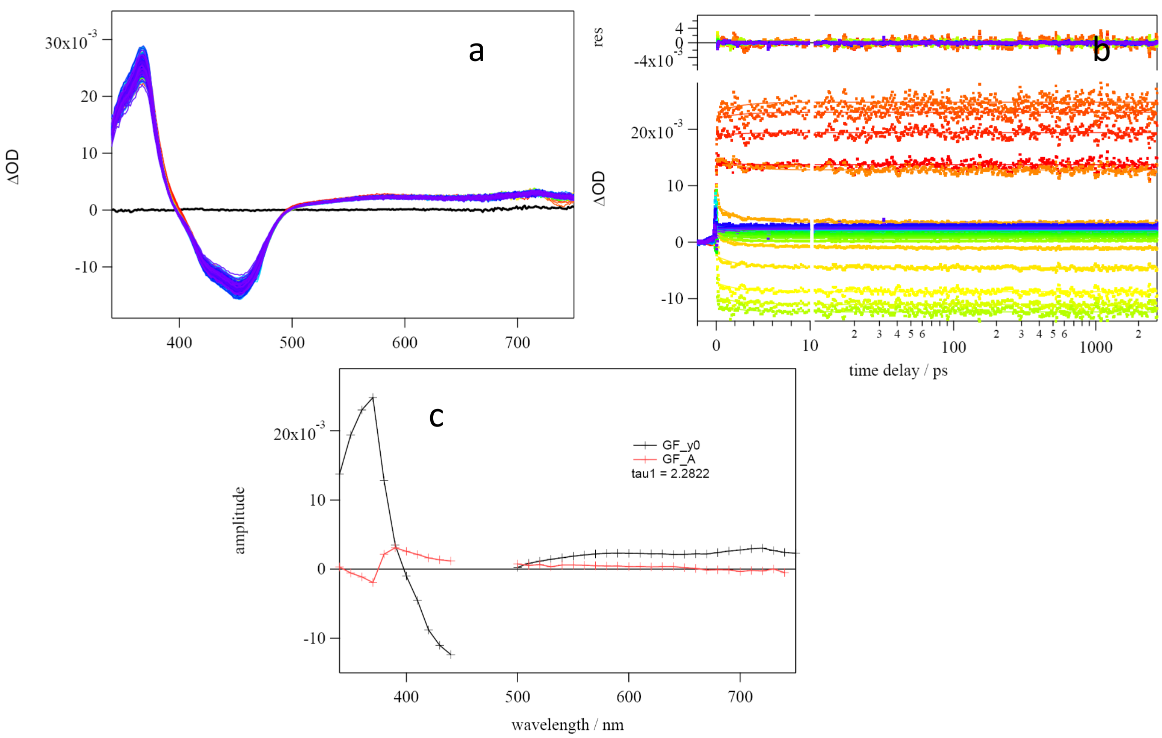

Fig. S18 (a) Observed fs-TA spectra from 340 to 750 nm at various time delays from τ = 0.2 (red) to τ = 2700 ps (blue), and pre time zero τ = -0.2 ps (black) for a *ca*. 120 M solution of (**Ru-2**) in CH_3CN solution using λ_{ex} = 470 nm. (b) Corresponding kinetic plots and global fit of observed fs-TA signals from τ = 0.2 to τ = 2700 ps in 10 nm wavelength increments from 340 nm (red) to 750 nm (blue). NB: data between 450-490 nm was excluded due to the presence of scattered laser excitation, and note the change to log scale from τ > 10 ps on the *x*-axis. (c) Deconvolution of globally fitted kinetic data into Decay Associated Difference Spectra (DADS).

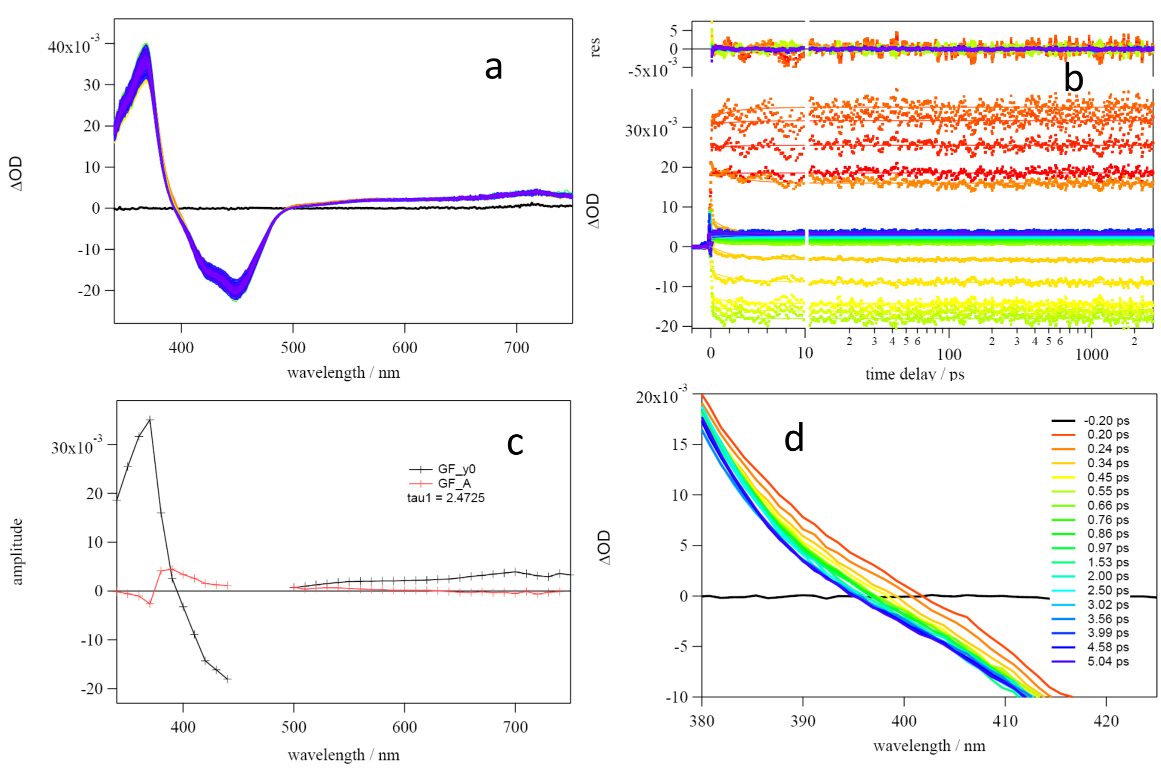

Fig. S19 (a) Observed fs-TA spectra from 340 to 750 nm at various time delays from τ= 0.2 (red) to τ = 2700 ps (blue), and pre time zero τ = -0.2 ps (black) for a *ca*. 160 M solution of $[Ru(bpy)_3]^{2+}$ in CH_3CN solution using λ_{ex} = 470 nm. (b) Corresponding kinetic plots and global fit of observed fs-TA signals from τ = 0.2 to τ = 2700 ps in 10 nm wavelength increments from 340 nm (red) to 750 nm (blue). NB: data between 450-490 nm was excluded due to the presence of scattered laser excitation, and note the change to log scale from τ > 10 ps on the x-axis. (c) Deconvolution of globally fitted kinetic data into Decay Associated Difference Spectra (DADS). (d) Expansion of fs-TA data showing blue shift of 370 nm ESA feature over first 5 ps due to vibrational cooling of rapidly formed ^{3}MLCT excited state (see text).

9.0 Changes of emission intensity of DPA upon the addition of NO

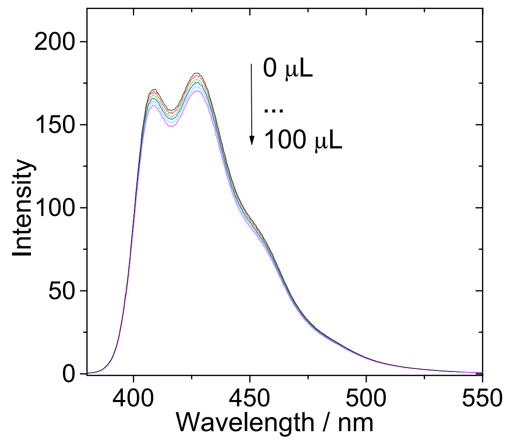

Fig. S20 Changes of emission spectrum of DPA upon the addition of NO (saturated solution in CH_3CN). $c = 1.0 \times 10^{-5}$ M, $\lambda_{ex} = 350$ nm, In CH_3CN, 20 °C.

10.0 Changes of emission intensity of Ru-1 and Ru-2 upon the addition of NO

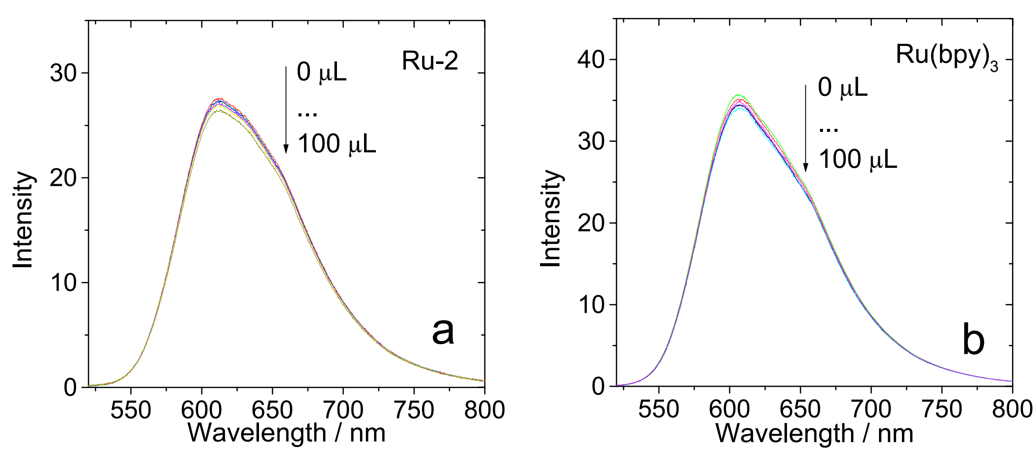

Fig. S21 Changes of emission spectrum of **Ru-2** (a) and $[Ru(bpy)_3]Cl_2$ (b) upon the addition of NO (saturated solution in CH_3CN). $c = 1.0 \times 10^{-5}$ M, $\lambda_{ex} = 445$ nm, In deaerated CH_3CN, 20 °C.

11.0 HPLC analysis of the complexes Ru-1, Ru-2 and the reaction mixture of Ru-1 + NO

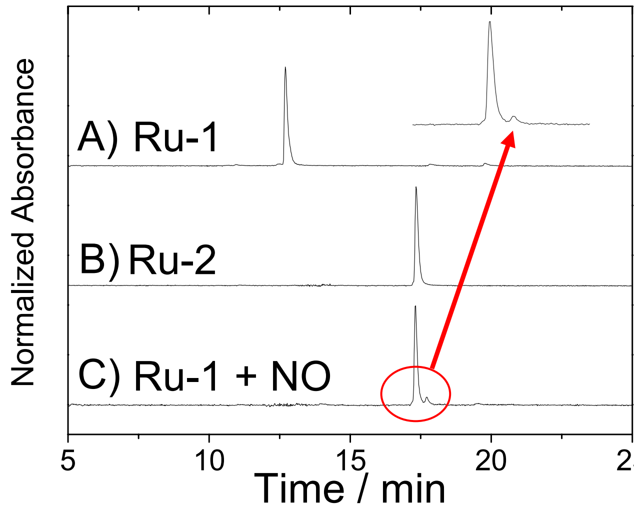

Fig. S22 HPLC analysis of the complexes **Ru-1**, **Ru-2** and the reaction mixture of **Ru-1** + **NO**. Line A: pure **Ru-1** solution (1×10^{-3} M); Line B: pure **Ru-2** solution (1×10^{-3} M); Line C: the reaction mixture of **Ru-1** + **NO** (NO saturated solution) (1×10^{-3} M).

12.0 The TTA upconversion of Ru-1 and Ru-2 upon the addition of NO

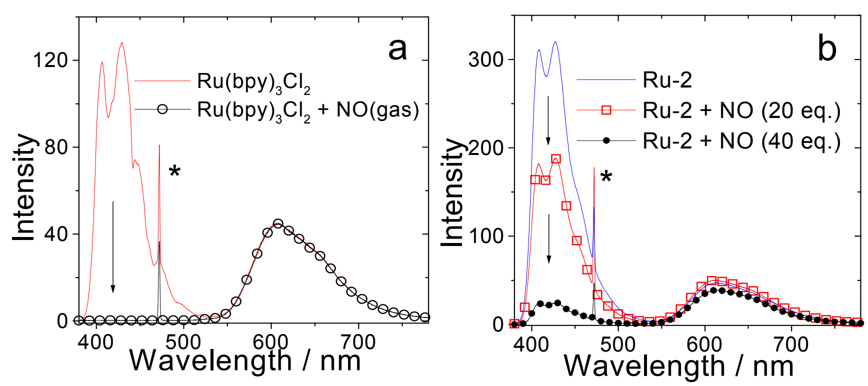

Fig. S23 The upconversion intensity of **Ru(bpy)$_3$Cl$_2$** and **Ru-2** upon the addition of NO (saturated solution in CH_3CN or pure NO gas). (a) Purging of the solution with pure NO gas for 10 second, *c*(**DPA**) = 2.0×10^{-4} M; (b) NO saturated solution in CH_3CN was added, *c*(**DPA**) = 4.0×10^{-4} M. *c*(Sensitizers) = 2.0×10^{-5} M. λ_{ex} = 473 nm (4.8 mW). In deaerated CH_3CN, 20 °C.

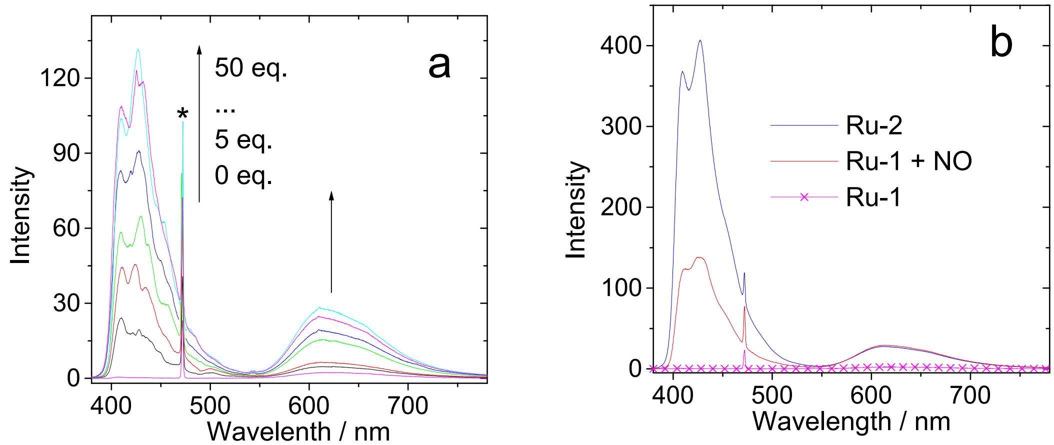

Fig. S24 Upconverted fluorescence intensity upon the addition of NO ($NaNO_2$ + HCl solution). (a) **Ru-1** as photosensitizer, the detail procedure was that: different equivalent of $NaNO_2$ + HCl solution was added into **Ru-1** solution (in CH_3CN) at 0 °C for 10 min, then remove the solvent and dissolve the mixture in fresh CH_3CN for the TTA upconversion measurement; (b) the upconversion intensity of **Ru-2**, **Ru-1** and **Ru-1** in the presence of NO ($NaNO_2$ + HCl solution). λ_{ex} = 473 nm (laser power: 4.8 mW). c(**sensitizers**) = 2.0×10^{-5} M, c(DPA) = 4.0×10^{-4} M, in deaerated CH_3CN, 20 °C.

13.0 The changes of phosphorescence intensity of the photosensitizers upon the addition of DPA

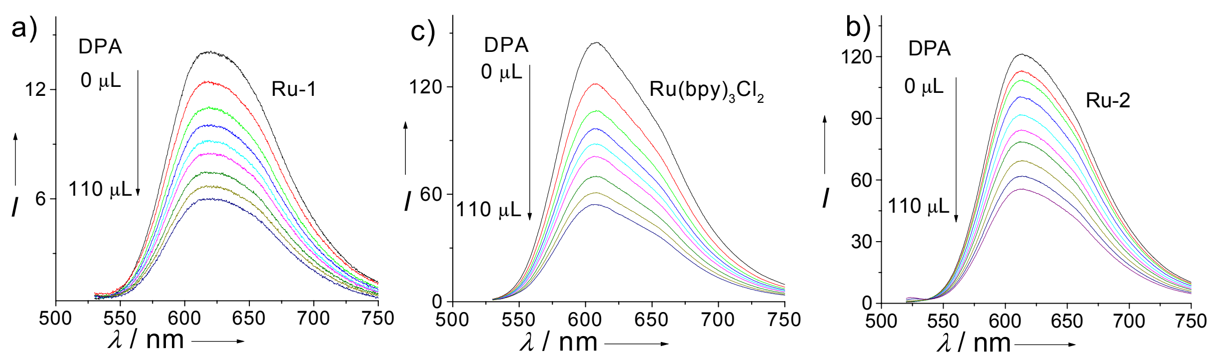

Fig. S25. (a), (b) and (c) the changes of phosphorescence intensity upon the addition of **DPA,** c (**DPA**) = 1.0×10^{-2} M, c (**Photosensitizers**) = 1.0×10^{-5} M, λ_{ex} = 445 nm in CH_3CN, 20 °C.

The bimolecular quenching efficiency (f_Q) was also studied. Stern-Volmer quenching constants were calculated as $K_{SV} = 3.36 \times 10^3$ M^{-1} for **Ru-1**. The bimolecular quenching constant was calculated as $k_q = K_{SV}/\tau_0 = 4.95 \times 10^9$ M^{-1} s^{-1}, where τ_0 is the triplet state lifetime of the triplet energy donor (737.6 ns). In order to study the quenching efficiency, which is given by $f_Q = k_q/k_0$, where k_0 is the diffusion-controlled bimolecular quenching rating constants, we used the Smoluchowski equation,

$$k_0 = 4\pi RND/1000 = \frac{4\pi N}{1000}\left(R_f + R_q\right)\left(D_f + D_q\right) \qquad \text{(Eq. 3)}$$

where D is the sum of the diffusion coefficients of the energy donor (D_f) and quencher (D_q), N is Avogadro's number and R is the collision radius obtained as the sum of the molecule radii of the energy donor (R_f) and the quencher (R_q). Diffusion coefficients can be obtained from Stokes-Einstein equation:

$$D = k\mathrm{T}/6\pi\eta R \qquad \text{(Eq. 4)}$$

where k is Boltzmann's constant, η is the solvent viscosity and R is the molecule radius.

14.0 Decay curves of Ru-1 in aerated CH_3CN

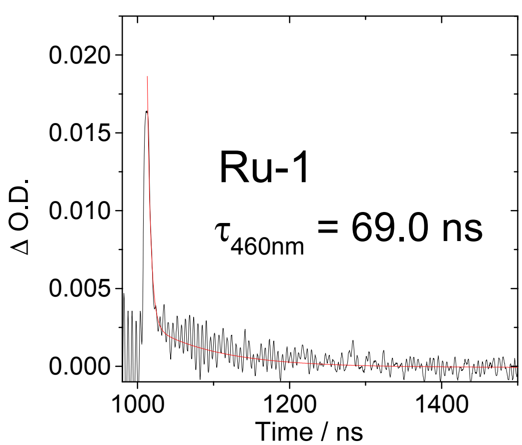

Fig. S26 Decay curves of **Ru-1** at 460 nm after pulsed laser excitation in aerated CH_3CN. c [**Ru-1**] = 1.0×10^{-5} M, λ_{ex} = 445 nm.

15.0 Calculation of triplet state quantum yield

Table S1. The Parameter Related to Calculate the Triplet State Quantum Yields. [a]

	ε [b]	ΔA [c]	Φ_T(%) [d]
Ru-1	1.36	– 0.0017	22.2 ± 5
Ru-2	1.36	– 0.0065	85.5 ± 5
Ru(bpy)$_3$Cl$_2$	1.26	– 0.0071	100.0

[a] In deaerated CH_3CN, [b] Molar absorption coefficient. ε : 10^4 M^{-1} cm^{-1}. [c] The O.D. value of the triplet transient difference absorption spectrum at 450 nm. [d] The triplet state quantum yield.

16.0 Cyclic voltammogram of Ru-1, Ru-2 and Ru(bpy)$_3$Cl$_2$ in deaerated CH_3CN

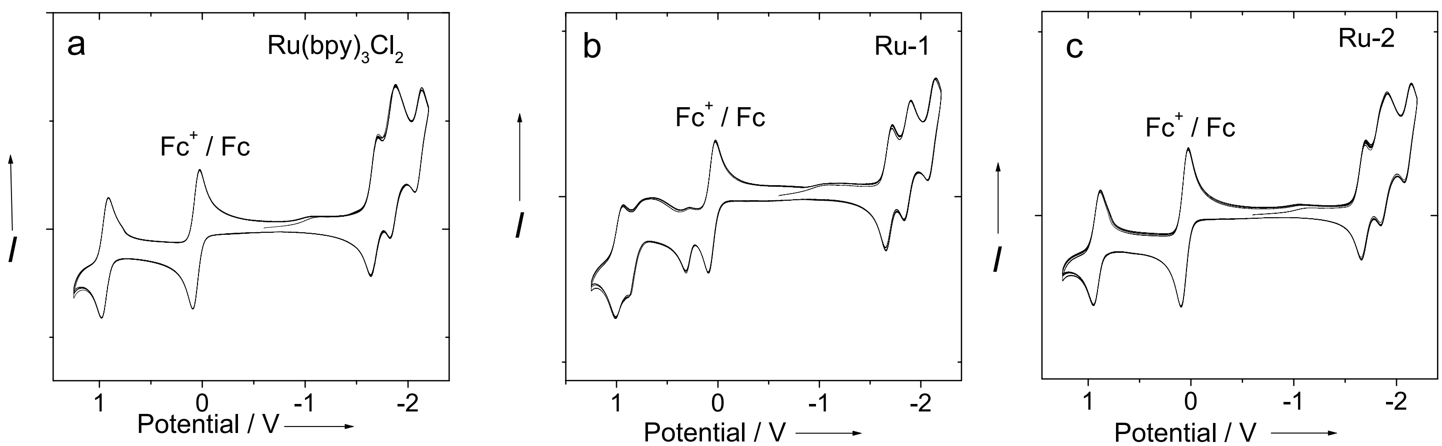

Fig. S27. Cyclic voltammogram of **Ru-1**, **Ru-2** and **Ru(bpy)$_3$Cl$_2$** in deaerated CH_3CN containing 0.10 M Bu_4NPF_6 as supporting electrode and with Ag/$AgNO_3$ reference electrode. Scan rates: 0.1 V/s, three cycles. Ferrocene (Fc) was used as internal reference, 20 °C.

Rehm-Weller equation (Eqs. 1 and 2.),[63,64]

$$\Delta G_{\mathrm{CS}} = e[E_{OX} - E_{RED}] - E_{00} + \Delta G_{\mathrm{S}} \quad \text{(Eq. 1)}$$

$$\Delta G_{\mathrm{S}} = -\frac{e^2}{4\pi\varepsilon_{\mathrm{S}}\varepsilon_0 R_{\mathrm{CC}}} - \frac{e^2}{8\pi\varepsilon_0}\left(\frac{1}{R_D}+\frac{1}{R_{\mathrm{A}}}\right)\left(\frac{1}{\varepsilon_{REF}}-\frac{1}{\varepsilon_S}\right) \qquad \text{(Eq. 2)}$$

where ΔG_{S} is the static Coulombic energy, which is described by Eq. 2, e is the electronic charge, E_{OX} is the half-wave potential for mono-electron oxidation of the electron-donor unit and E_{RED} is the half-wave potential for one-electron reduction of the electron-acceptor unit.

17.0 Simplified Jablonski diagram illustrating the photophysical processes

Scheme S2. Simplified Jablonski Diagram Illustrating the Photophysical Processes Involved in the NO-switched TTA Upconversion, (a) **Ru-1** as Photosensitizer, (b) **Ru-2** as Photosensitizer. [a]

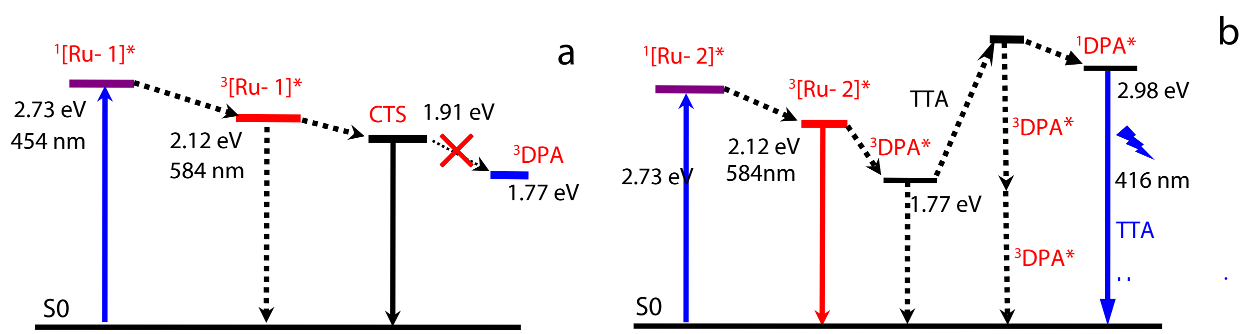

[a] The component at the excited state was designated with red color. The number of the superscript designated either the singlet or the triplet excited state. CH_3CN as the solvent.